Malaysian Journal of Science **25** (1): 115 – 127 (2006)

Finite Element Based Dynamic Characteristics of Journal Bearing in a New Two-Stroke Linear Generator Engine

M. M. Rahman* and **A. K. Ariffin**

Department of Mechanical and Materials Engineering,
Universiti Kebangsaan Malaysia (UKM), 43600 Bangi, Selangor, Malaysia
* mustafiz@eng.ukm.my
Received 24th January 2005, accepted in revised form 23rd December 2005.

ABSTRACT This paper presents the dynamic characteristics of hydrodynamic journal bearing in a new two-stroke linear generator engine to solve tribological problems considering constant viscosity of the lubrication using the finite element method. The tribological phenomenon of the sliding surfaces between connecting rod and bush may be among the most complex in the linear generator engine and could become even more severe with increasing the engine power. The friction between the connecting rod and bush significantly contributes to the power losses of the engine. On the basis of the finite element analysis theory, the Reynolds equation for dynamic loads is derived. The results represent the bearing characteristics, namely the variation of pressure along the circumference, effects of load-carrying capacity, frictional losses, and stiffness and damping coefficient with the eccentricity ratio and also presented the variation of eccentricity ratio with Sommerfeld number. Results from the numerical analysis indicated that the effect of load-carrying capacity, frictional losses strongly depends on the eccentricity ratio. It also shows that the dynamic characteristics, namely stiffness and damping coefficients also greatly depends upon the eccentricity ratio. This paper also investigated the performance characteristics of the journal bearing as well as on its stability.

(FEM, friction, journal bearing, stiffness coefficient, damping coefficient, lubrication)

ABSTRAK Kertas kerja ini membentangkan ciri-ciri hidrodinamik galas jurnal engin penjana linear baru bagi menyelesaikan masalah tribologi dengan mempertimbangkan pelinciran berkelikatan malar menggunakan kaedah unsur terhingga. Fenomena tribologi bagi permukaan bergelangsar antara rod penyambung dan galas berkemungkinan antara fenomena yang kompleks dalam enjin penjana linear dan akan semakin serius dengan peningkatan kuasa enjin. Geseran antara rod penyambung dan galas banyak menyumbang kepada kehilangan kuasa enjin. Dengan asas teori unsur terhingga, persamaan Reynolds bagi beban dinamik diterbitkan. Keputusan menerangkan ciri-ciri galas, iaitu variasi tekanan terhadap lilitan, kesan muatan beban angkut, kehilangan geseran, pekali kekakuan dan redaman dengan nisbah kesipian dan juga variasi nisbah kesipian dengan nombor Sommerfeld. Keputusan dari analisis berangka menunjukkan kesan muatan beban angkut, kehilangan geseran sangat bergantung kepada nisbah kesipian. Adalah ditunjukkan bahawa ciri-ciri dinamik iaitu pekali kekakuan dan redaman bergantung kepada nisbah kesipian. Kertas ini juga menerangkan kajian ciri-ciri prestasi galas jurnal serta kestabilannya.

(FEM, geseran, galas jurnal, pekali kekakuan, pekali redaman, pelinciran)

INTRODUCTION

The free piston engine is unique in that there is no crankshaft, or any of the mechanical linkages typically found in reciprocating internal combustion engines. Because of this the piston oscillates freely within the cylinder. The free-piston two-stroke linear generator (LG) engine is the most recent application of the free-piston concept. Hybrid vehicles are presumed to be the ultimate use for these engines [1]. Piston motion in LG engine is predominately linear. Consequently transverse piston loads are nearly absent and piston-cylinder friction reduced. Schematic diagram of linear generator engine is shown in Figure 1. Journal bearings are used to provide radial location for shaft in LG engine as shown in Figure 1. The bearing choice depends

on the application where the dynamic behavior needs to be considered [2]. When oil lubricated journal bearing operate at high speed, thermal effects become important.

In the journal bearing tribology, three lubrication regimes are often defined namely boundary, mixed and full film lubrication. These lubrication regimes can be explained by the Stribeck diagram obtained by McKee *et al.* [3] as shown in Figure 2. This diagram presents the change in the coefficient of friction, against the bearing parameter, $\eta U/RP$, where η is the dynamic viscosity of the lubrication (N-s/m^2), U is the axial velocity (m/s), R is the radius of the shaft, and P is the nominal bearing pressure (N/m^2). Since it defines the stability of lubrication and helps one to understand the lubrication regimes, it may be used as a rough design parameter or as an approximate means for quickly deciding if the bearing is operating near a danger zone. However, it does not include the eccentricity ratio (clearance ratio), $\varepsilon=c/R$ where c is the radial clearance. In view of the above, a more comprehensive parameter, the Sommerfeld Number (S) was used in this study to take into account the variables generally specified by the designer. Tribological properties of the journal bearings were then obtained via the graphics plotted using the friction factor (f), versus the Sommerfeld Number (S).

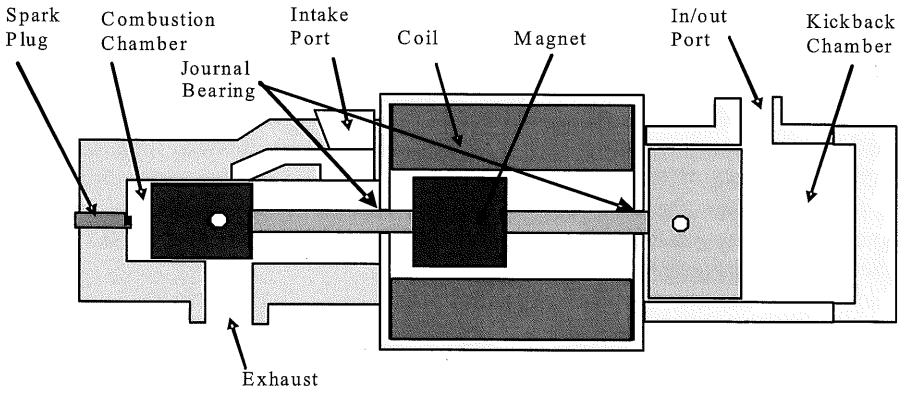

Figure 1. Schematic Diagram of Linear Generator Engine

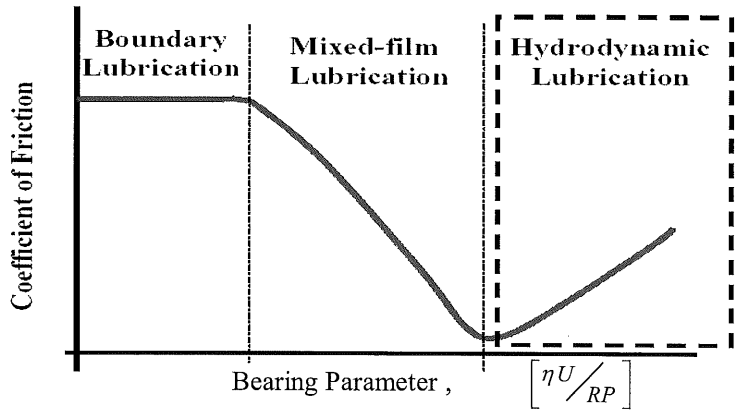

Figure 2. Typical Stribeck Diagram

The performance of the hydrodynamic journal bearings using the assumption of continuous lubricating film and isothermal conditions have been extensively studied by many investigators [4-5]. During the last few decades, considerable work have been carried out and reported in the area of journal bearings. Stout and Rowe [6-7] presented a useful study relating to the selection

of configuration geometry, control devices and material for both gas and liquid fed journal bearing along with an additional guidance concerning the achievement of total system reliability. Xu [8] carried out an experimental work study to the performance of hybrid journal bearing having various bearing configurations including the double–row slot-entry journal bearing. The results for load carrying capacity and for the stiffness and damping coefficient with respect to different eccentricity ratios were reported.

The influence of the roughness parameter and the roughness patterns on the steady state and dynamic characteristics of hydrodynamic journal bearings with rough surfaces by Turaga *et al.* [9] was investigated. The surface roughness effects on the pure squeeze-film behavior of a long partial journal bearing operating under a time-depending oscillating load were analyzed by Lin et al. [10]. Cheng and Rowe [11] concentrated on computerized selection method for the bearing type and configuration, fluid feeding device, bearing material and production techniques concerning externally pressurized journal bearings including the slot-entry journal bearings. Chun and Ha [12] showed numerically that heat convection played only a small role in determining friction and load under the no mixing condition. However, so far, the detailed investigation of the performance parameters of hydrodynamic journal bearing with linear motion has not been studied yet. In this paper, a journal bearing of finite width is analyzed. This paper studies the dynamic characteristics of journal bearing configurations using the finite element method. The study is expected to be useful to bearing designers. A fast and accurate journal bearing hydrodynamic analysis is presented based on a finite element formulation. The governing equations for the oil film pressure, stiffness and damping characteristics are solved using the finite element approach.

THEORETICAL ANALYSIS

A local coordinate system can be set up in the region between the bush and the journal surfaces as shown in Figure 3. In 1886, Osborne Reynolds derived the following equation from the Navier-stokes equation and a coordinate system similar to the one shown in Figure 3.

$$\frac{\partial}{\partial x}\left(\frac{h^3}{\mu}\frac{\partial P}{\partial x}\right)+\frac{\partial}{\partial z}\left(\frac{h^3}{\mu}\frac{\partial P}{\partial z}\right)=6U\frac{\partial h}{\partial x} \quad (1)$$

where P = pressure and μ = lubricant viscosity.

The derivation of Equation (1) can be referred the the articles published by Cameron [13] and Hamrock [14]. Reynolds' equation can be solved over the domain of bush surface in the journal bearing to give the pressure distribution. A typical meshed bearing surface with essential pressure boundary conditions is shown in Figure 4.

The domain has been meshed using MSC.MARC element type 39, which is an arbitrary four-node isoparametric quadrilateral element with bilinear pressure interpolation that has been used for planar lubrication applications. Figure 5 shows the 4-node isoparametric quadrilateral element. As this element uses bilinear interpolation functions, the pressure gradients tend to be constant throughout the element. The connectivity of this element is formed using four-point Gaussian integration.

In the finite element method, basis functions are used to approximate the exact solution to a differential equation. These basis functions are defined over simple elements which comprise a mesh of a particular domain. Accompanying these basis function are unknown coefficients which can be obtained by setting the weighted integral of a residual to be equal to zero [15].

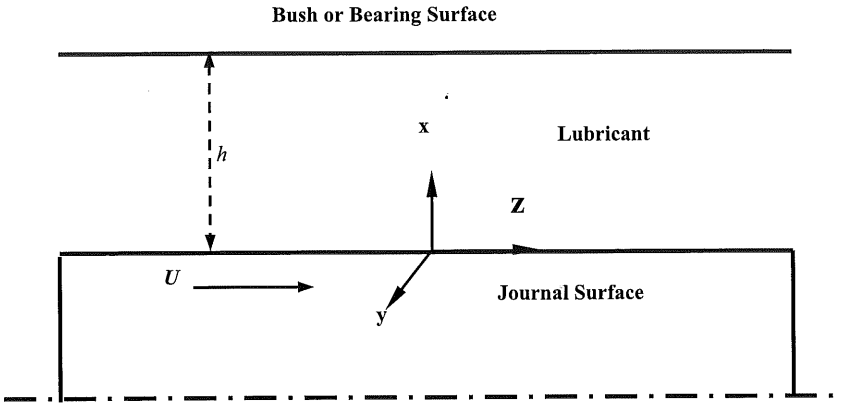

Figure 3. Co-ordinate system for Reynolds' equation

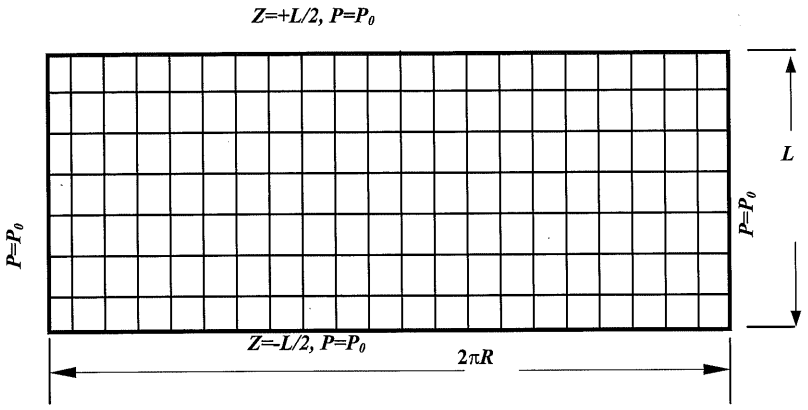

Figure 4. Typical meshed bearing surface with essential pressure boundary conditions

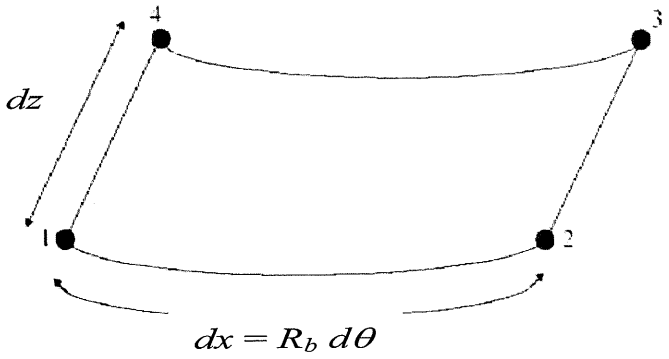

Figure 5. 4 node isoparametric Quadrilateral Element

The dimension of the journal bearing and the lubrication properties are listed in the Table 1.

Table 1. The Dimension of the Journal Bearing and the Lubrication Properties

Description of items and symbol	Quantities and unit
Diameter of the journal (D_j)	25 mm
Length of the Bush(L)	30 mm
Radial clearance (c)	20 μm
Axial velocity of shaft (U)	10.0 m/sec
Viscosity of the lubricant(η)	0.0153 N-sec/m^2
Density of the Lubricant(μ)	880 kg/m^3
Supply pressure of the lubricant(P_0)	1.53 MPa
Supply temperature of the lubricant(T_s)	40°C

Bearing Characteristics

The load-carrying capacity, W is defined as

$$W = \sqrt{F_x^{\,2} + F_y^{\,2}} \quad \text{and} \quad \tan\delta = \frac{F_y}{F_x} \tag{2}$$

The friction force can be obtained by integrating the shear stress around the journal surface. The shear stress at the journal surface [12] can be obtained using the following equation.

$$\tau = \mu \left.\frac{\partial u}{\partial y}\right|_{y=0} - \eta \left.\frac{\partial^3 u}{\partial y^3}\right|_{y=h} = \mu\left(\frac{U}{h} + \frac{h}{2\mu}\frac{\partial P}{\partial x}\right) \tag{3}$$

Thus the friction force is

$$F_f = \frac{\eta R_b L U}{c}\frac{2\pi}{\sqrt{1-\varepsilon^2}} + \frac{e}{2R_b} W \sin\delta \tag{4}$$

So that the friction coefficient can be calculated from the relation

$$c_f = \frac{F_f}{W} \tag{5}$$

The power losses of the journal bearing is obtained by

$$P = F_f \times U \tag{6}$$

To model the dynamic behaviour of a system, a model must be assumed for the bearings which support the shaft. Unfortunately, the force versus displacement characteristics of hydrodynamic bearings are noticeably non-linear. Since in journal bearings the directions of external load and corresponding movement of journal center do not generally coincide, the state of equilibrium of a shaft supported by journal bearings becomes unstable under certain conditions. When the journal vibrates, squeeze film pressure is generated. This pressure gives rise to spring and damping forces of the oil film and therefore influences the stability of the shaft–bearing system. The components of the oil film force can be written as:

$$F_x = F_x(x, y, \dot{x}, \dot{y}), \quad F_y = F_y(x, y, \dot{x}, \dot{y}) \tag{7}$$

These non-linear functions can be expressed as a linear function, for small amplitude of vibration, of the displacement and velocity of the journal center by using a first-order Taylor series expansion. The force system has the following form:

$$\begin{aligned} F_x &= F_{x0} + \left(\frac{\partial F_x}{\partial x}\right)_0 \Delta x + \left(\frac{\partial F_x}{\partial y}\right)_0 \Delta y + \left(\frac{\partial F_x}{\partial \dot{x}}\right)_0 \Delta \dot{x} + \left(\frac{\partial F_x}{\partial \dot{y}}\right)_0 \Delta \dot{y} \\ F_y &= F_{y0} + \left(\frac{\partial F_y}{\partial x}\right)_0 \Delta x + \left(\frac{\partial F_y}{\partial y}\right)_0 \Delta y + \left(\frac{\partial F_y}{\partial \dot{x}}\right)_0 \Delta \dot{x} + \left(\frac{\partial F_y}{\partial \dot{y}}\right)_0 \Delta \dot{y} \end{aligned} \tag{8}$$

where subscript (0) denotes that the load components and partial derivatives are evaluated at the equilibrium position. The linear stiffness and damping coefficients are then defined as:

$$K_{xx} = \left(\frac{\partial F_x}{\partial x}\right)_0, K_{xy} = \left(\frac{\partial F_x}{\partial y}\right)_0, K_{yx} = \left(\frac{\partial F_y}{\partial x}\right)_0, K_{yy} = \left(\frac{\partial F_y}{\partial y}\right)_0$$

$$B_{xx} = \left(\frac{\partial F_x}{\partial \dot{x}}\right)_0, B_{xy} = \left(\frac{\partial F_x}{\partial \dot{y}}\right)_0, B_{yx} = \left(\frac{\partial F_y}{\partial \dot{x}}\right)_0, B_{yy} = \left(\frac{\partial F_y}{\partial \dot{y}}\right)_0$$

The dynamic equilibrium equations of the journal bearing using the finite element method are written as :

$$[B]\{\dot{x}\} + [K]\{x\} = \{F(x, y)\} \tag{9}$$

The effect of dynamic coefficient will be reflected on the stability of the shaft-bearing system. According to the work of Lund [17], the critical speed is given as:

$$M_{cr} = \frac{K_0 (B_{YY} B_{xx} - B_{xy} B_{yx})}{(K_{xx} - K_0)(K_{yy} - K_o) - K_{xy} K_{yx}} \quad (10)$$

where

$$K_0 = \frac{K_{xx} B_{yy} + K_{yy} B_{xx} - K_{xy} B_{yx} - K_{yx} B_{xy}}{B_{yy} + B_{xx}}$$

The non-dimensional critical speed (ϖ) of the shaft is then given by:

$$\varpi = \omega_{cr} \sqrt{\frac{mc}{w}} = \sqrt{M_{cr}} \quad (11)$$

This critical speed will be used for expressing the threshold stability of the shaft-bearing system.

Numerical Scheme

MSC.MARC is used for solving steady state lubrication problems; the incremental procedure analyzes a sequence of different lubrication film profiles. The nodal point data consists of pressures, equivalent nodal mass flux at fixed boundary points, or residuals at points where no boundary conditions are applied. In addition, the $h(\phi) = (1 - \varepsilon \cos\phi)10^{-6} m$. The flow chart of journal bearing analysis is shown in Figure 6.

This bearing analysis deals only steady state and does not include the analysis of transient lubrication phenomena. The incrementation procedure is only meant to analyze a sequence of film profiles. No nonlinearities are involved; each increment is solved in a single step without iteration. To calculate the reaction forces that act on the bearing structure, MSC.MARC requires information about the spatial orientation of the lubrication. This information is not contained in the finite element model because of the planar representation of the lubrication. Therefore, it is necessary to define the direction cosines of the unit normal vector that is perpendicular to the lubrication on a nodal basis in user subroutine UBEAR [16] which is called for each node. The calculation of bearing dynamic characteristics i.e. damping and stiffness properties is performed in subincrements based on a specified change in lubricant film thickness. The variation of the film thickness is again specified in subroutine UTHICK. In total, 4 subincrements are specified. A displacement of shaft center of 1.0×10^{-7} m in each global direction is given for both damping and stiffness properties.

program automatically integrates the calculated pressure distribution over the entire region to obtain consistent equivalent nodal forces. This integration is only performed in regions where the pressure exceeds the cavitation pressure. It is assumed that atmospheric pressure is acting on the end faces of the bearing system.

The FIXED PRESSURE option is used to specify these boundary conditions. Tying (multipoint constraint) was applied to the nodal pressure at both sides of the mesh to simulate the continuous pressure distribution in the circumferential direction. The variation of the lubrication thickness over the mesh due to the eccentric position of the shaft is specified in user subroutine UTHICK [16]. User subroutine UTHICK allows to define or to redefine previously specified nodal thickness. It is called for each node in the mesh. This subroutine can be used to define thickness increments in incremental analysis or within subincrements when evaluating damping and/or stiffness coefficients. This subroutine determines the nodal thickness values using the expression of

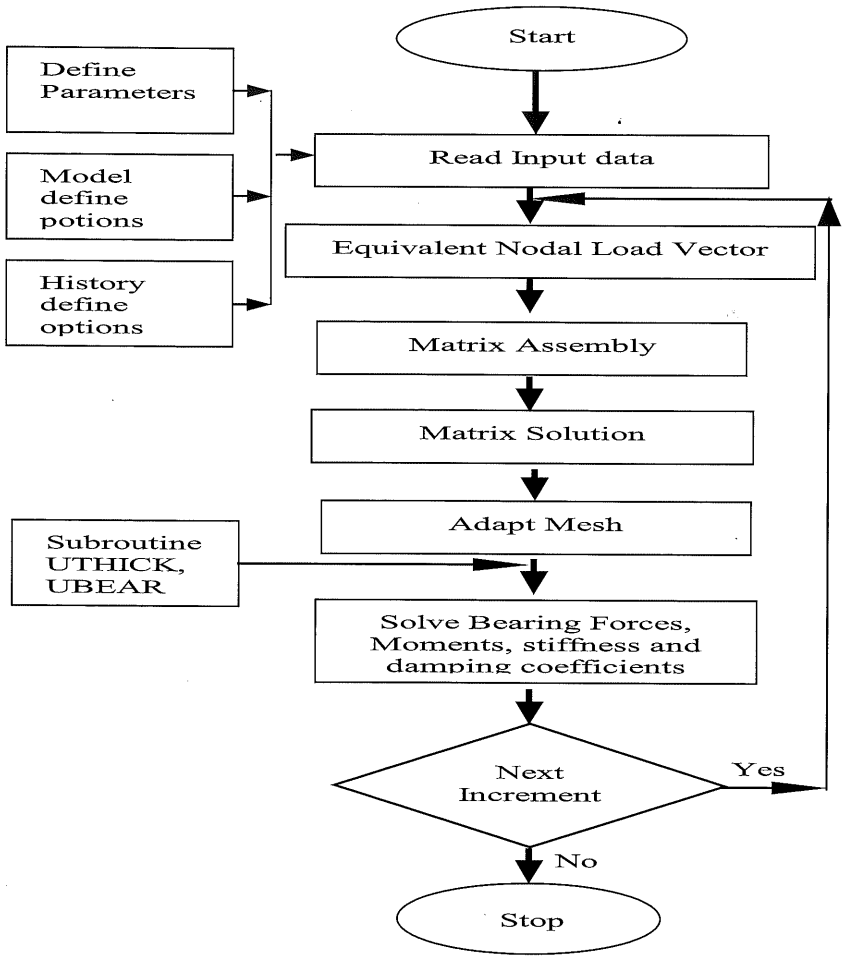

Figure 6. Flow Chart of Journal bearing analysis

RESULTS AND DISCUSSION

The results from finite element analysis of the Reynolds equation have been presented for a complete incompressible journal bearing. These results focused on a complete journal bearing and a complete range of eccentricity ratios or minimum film thickness. The performances parameters presented for these range of operating parameters are dimensionless load, friction of coefficient, power loss etc. These parameters have been presented in the form of figures that can be easily used for designing plain journal bearing in the linear generator engine. The terms S is one of the several forms of the Sommerfeld number ($S = wc^2 / \eta LUR_b^2$), a dimensionless load carrying capacity. Figure 7 shows the variation of eccentricity ratio with dimensionless load parameter (Sommerfeld Number) that obtained by means of finite element method for linear velocity 10 m/s for complete incompressible film journal bearing. As shown in this figure non-dimensional bearing parameter varies as a function of non-dimensional eccentricity ratio can be displayed. It can be seen that velocities tend to be higher and loads lower at the right, and the opposite phenomena holds at the left. No analysis of journal bearing can be considered complete until an evaluation of the probable friction and power has been made. This estimate is then weighed against the expected heat dissipating capacity of the bearing. The variation of non-dimensional frictional force with the eccentricity ratio for different velocity is shown in Figure 8.

Variation of friction force slightly increases when the eccentricity ratio increases. When is large or is near to 1.0, the non-dimensional friction force

increases rapidly. Variation of load carrying capacity with eccentricity ratio is also shown in Figure 9. It can be seen that the load carrying capacity parabolically increases with increase of the eccentricity ratio. The pressure contour field in lubrication of journal bearing is shown in Figure 10 at linear velocity 10 m/s, eccentricity ratio 0.5 and increment 0. The pressure distribution for the given bearing system is calculated in increment 0. Figure 11 shows a path plot of the calculated pressure distribution along the circumference at half width position. This figure shows that the pressure distribution is skewed symmetrically with the numerical values of the maximum and minimum pressures.

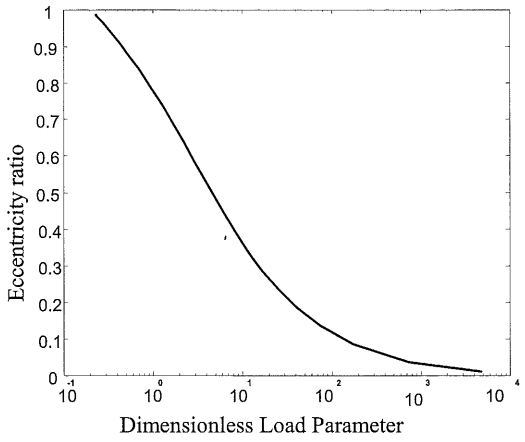

Figure 7. Variation of Eccentricity Ratio with Dimensionless Load Parameter

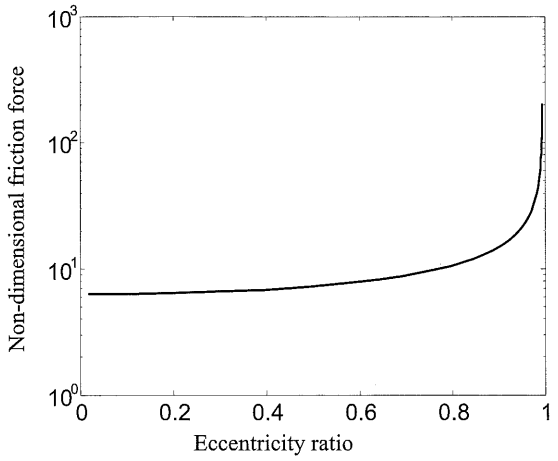

Figure 8. Variation of Frictional Force with Eccentricity Ratio

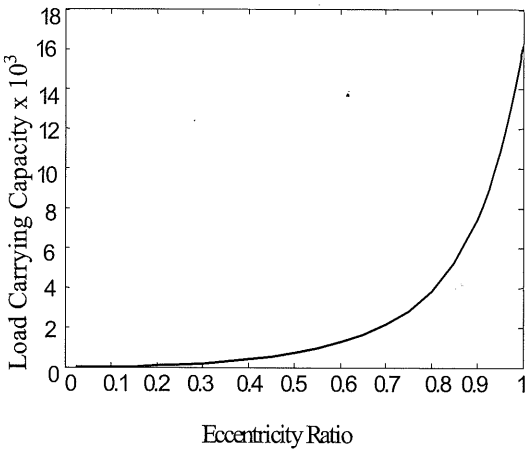

Figure 9. Variation of Load Carrying Capacity with the Eccentricity Ratio.

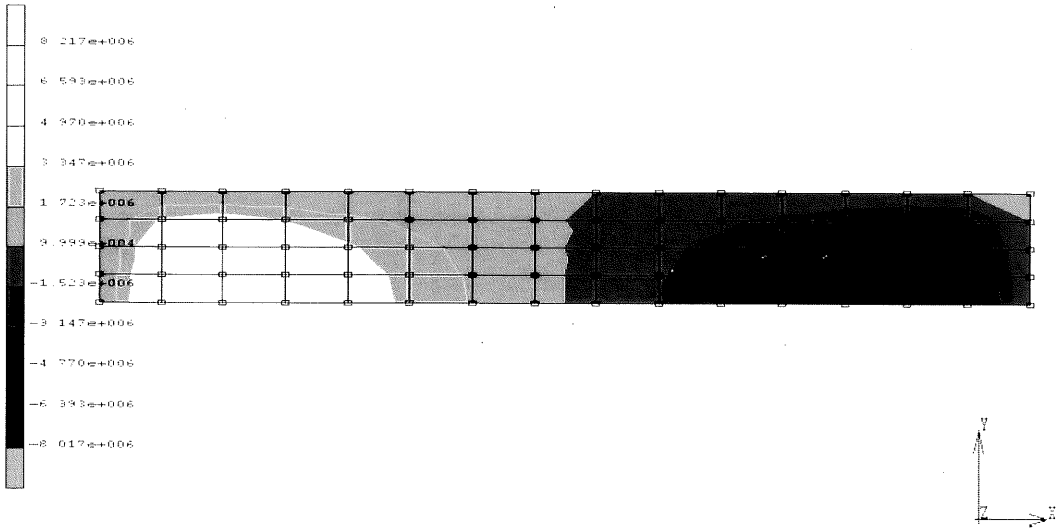

Figure 10. Pressure contour of journal bearing

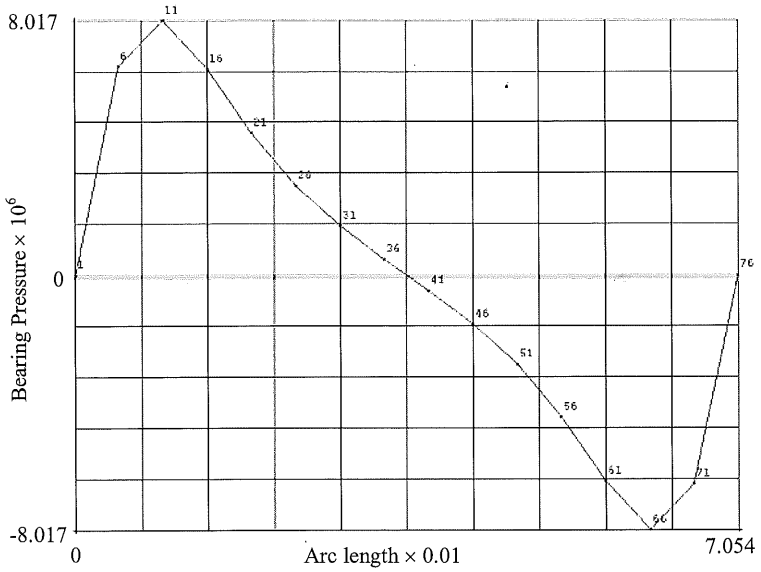

Figure 11. Path Plot of Pressure Distribution Along Circumference at Half Width Position

Variations of stiffness coefficients K_{xx}, K_{xy}, K_{yx}, K_{yy} with eccentricity ratio are presented in Figure 12 and 13. The figure shows that the stiffness generally decreases as a journal eccentricity increases. However Figure 13 shows K_{yx} and K_{yy} increases due to existence couple stresses at high values of eccentricity ratio. This may be explained by the fact that a thinner oil film would inherently deform less than a thicker oil film. The figure clearly shows that couple stiffness coefficient K_{yx} suddenly decreases and then increases with increases of eccentricity ratio and also happens in direct vertical coefficient. Figures 14 and 15 show variation of the damping coefficients with the eccentricity ratio. It shows that the direct damping coefficient B_{yy} is not affected throughout the range. However, The direct horizontal damping coefficient B_{xx} and the cross-coupling damping coefficients B_{xy} and B_{yx} are greatly influenced with the eccentricity ratio. According to the obtained stiffness and damping coefficients, the stability limit of the shaft-bearing system is determined and plotted in Figure 16. It shows variation of the non-dimensional critical speed with the eccentricity ratio. The shaft is stable for speeds less than the critical value. The degree of stability or instability can be indicated by the margin of separation between the journal operating speed and critical speed. It is known that the system instability is associated with the cross-coupling coefficient K_{yx}. The Figure 13 shows a slight destabilizing effect with at very low and high values of eccentricity ratio. At high eccentricity ratio the hydrodynamic effect is the major effect. The Figure 16 also shows the system is always stable.

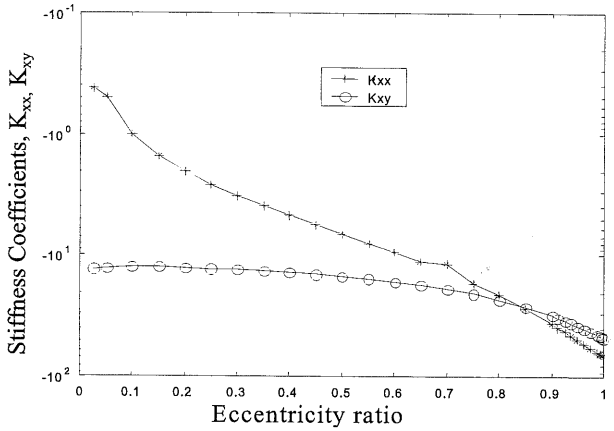

Figure 12. Variations of Stiffness Coefficients K_{xx} and K_{xy} with the Eccentricity Ratio

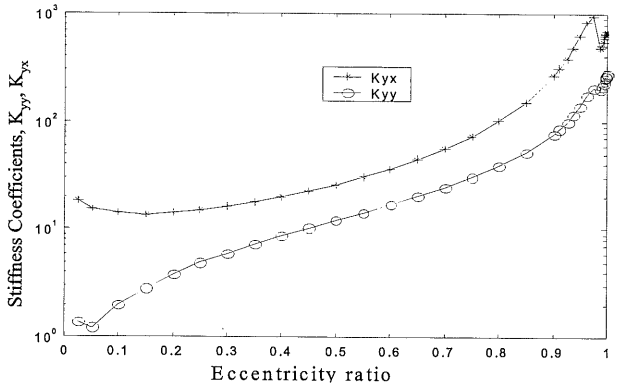

Figure 13. Variation of Stiffness Coefficients K_{yx}, K_{yy} versus the Eccentricity Ratio

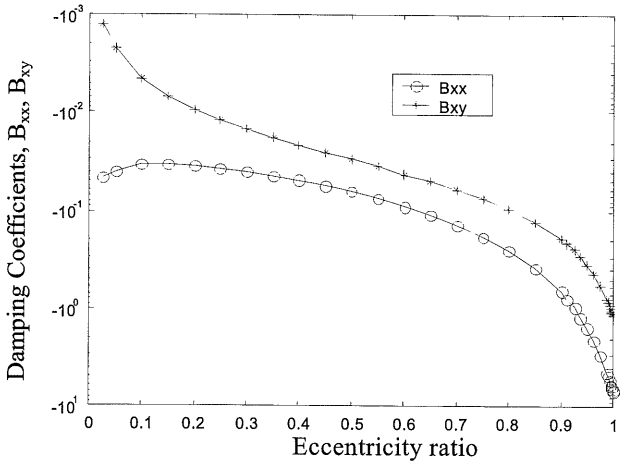

Figure 14. Variations of Damping Coefficients B_{xx} and B_{xy} with Eccentricity Ratio

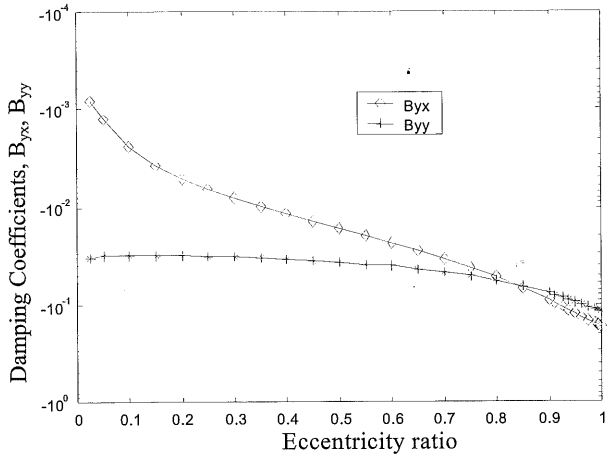

Figure 15. Variations of Damping Coefficients B_{yx} and B_{yy} with Eccentricity Ratio

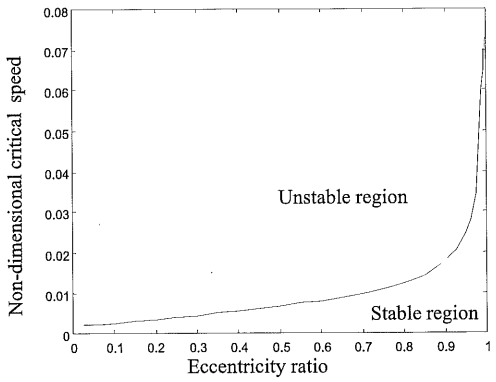

Figure 16. The effect of the Critical Speed versus Eccentricity Ratio

CONCLUSION

On the basis of the results presented in this paper, the following conclusions have been drawn.

- The non-dimensional friction force rapidly increases with large values of non-dimensional eccentricity ratio i.e. near 1.0. So the power loss depends on eccentricity ratio.
- The dimensionless load carrying capacity has significant influence on the eccentricity ratio of the hydrodynamic journal bearing.
- The stability threshold speed is a function of eccentricity ratio and also depends upon the values of stiffness and damping coefficients.
- The stiffness coefficients and the damping coefficients are greatly influenced by the eccentricity ratio except B_{yy}.
- The importance of the eccentricity ratio can be seen by the FEM analysis the lubrication model described above i.e. when the eccentricity ratio is greater than a certain value, the effect of friction force or power loss should not be ignored.

Therefore the eccentricity ratio is important for thin film lubrication analysis and will be of guiding significance for hydrodynamic journal bearing.

Acknowledgements The authors would like to thank the Department of Mechanical and Materials Engineering, Universiti Kebangsaan Malaysia (UKM), Malaysia. The authors are very grateful to the Ministry of Science, Technology and Innovation under IRPA project no: 03-02-02-

0056 PR0025/04-03) for providing financial support.

REFERENCES

1. B.P. Van, N. Paradiso and S.S. Goldsborough. (1998). Homogeneous charge compression ignition with a free piston: A new approach to ideal Otto Cycle performance. *SAE Technical Paper 982484.*
2. D.R. Garner. (1980). *The Use of Design Procedures for Plain Bearings.* Industrial Tribology Unit, University of Leeds. LB495/81.
3. S.A. McKee and T.R. McKee. (1932). Journal bearing friction in the region of thin film lubrication. *SAE J.* **31**: 371 – 377.
4. A.A. Raimondi and J. Boyd. (1958). A Solution for the finite journal bearing and its application to analysis and design. *Trans. ASLE* **1**: 159 – 209.
5. A.Z. Szeri. (1980). *Tribology, Friction, Lubrication and Wear*, McGraw Hill, New York, pp. 55 - 101.
6. K.J. Stout and W.B. Rowe. (1974). Externally pressurized bearings-design for manufacturing. Part 1: Journal bearing selection. *Tribology International* **7** (3): 98 – 106.
7. K.J. Stout and W.B. Rowe. (1974). Externally pressurized bearings-design for manufacturing. Part 3: Design of liquid externally pressurized bearings for manufacturing including tolerancing procedure. *Tribology International* **7** (5): 195 – 212.
8. S. Xu. (1994). Experimental investigation of hybrid bearing, *STLE Tribology Transactions* **37** (2): 285 – 92.
9. R. Turaga, A.S. Sekhar and B.C. Majumdar. (1999). The effect of roughness parameter on the performance of hydrodynamic journal bearing with rough surfaces. *Tribology International* **32**: 231 – 6.
10. J.R. Lin, C.H. Hsu and C. Lai. (2002). Surface roughness effects on the oscillating squeeze-film behaviour of long partial journal bearing. *Computer and Structures* **80**: 297 – 303.
11. K. Cheng and W.B. Rowe. (1995). A selection strategy for the design of externally pressurized journal bearings. *Tribology International* **28** (7): 465 – 474.
12. S.M. Chun and D. Ha. (2001). Study on mixing flow effects in a high speed journal bearing. *Tribology International* **34** (6): 397 – 405.
13. A. Cameron. (1981). *Basic Lubrication Theory* (3rd Edition). Ellis Horwood Ltd. Publishers.
14. B.J. Hamrock. (1994). *Fundamental of Fluid Film Lubrication.* McGraw-Hill, New York,
15. J.N. Reddy (1993). *An Introduction to the Finite Element Method.*
16. *MSC.MARC User Subroutines and Special Routines, volume D*, version 2003, MSC. Software Corporation, USA.
17. J.W Lund. (1987). Review of the Concept of Dynamic Coefficients for Fluid Film Journal Bearings. *ASME Journal of Tribology* **109**: 37 – 41.